

Explainable Synthetic Image Detection through Diffusion Timestep Ensembling

Yixin Wu^{*}, Feiran Zhang^{*}, Tianyuan Shi^{*}, Ruicheng Yin, Zhenghua Wang, Zhenliang Gan,
Xiaohua Wang, Changze Lv, Xiaoqing Zheng[†], Xuanjing Huang

School of Computer Science, Fudan University, Shanghai, China
Shanghai Key Laboratory of Intelligent Information Processing

{yixinwu23}@m.fudan.edu.cn {zhengxq, xjhuang}@fudan.edu.cn

Abstract

Recent advances in diffusion models have enabled the creation of deceptively real images, posing significant security risks when misused. In this study, we reveal that natural and synthetic images exhibit distinct differences in the high-frequency domains of their Fourier power spectra after undergoing iterative noise perturbations through an inverse multi-step denoising process, suggesting that such noise can provide additional discriminative information for identifying synthetic images. Based on this observation, we propose a novel detection method that amplifies these differences by progressively adding noise to the original images across multiple timesteps, and train an ensemble of classifiers on these noised images. To enhance human comprehension, we introduce an explanation generation and refinement module to identify flaws located in AI-generated images. Additionally, we construct two new datasets, *GenHard* and *GenExplain*, derived from the *GenImage* benchmark, providing detection samples of greater difficulty and high-quality rationales for fake images. Extensive experiments show that our method achieves state-of-the-art performance with 98.91% and 95.89% detection accuracy on regular and harder samples, increasing a minimal of 2.51% and 3.46% compared to baselines. Furthermore, our method also generalizes effectively to images generated by other diffusion models. Our code and datasets will be made publicly available.

1. Introduction

With the booming development of diffusion models such as Stable Diffusion [26], DALL-E 3 [1] and Midjourney [21], the proliferation of artificially generated images has reached unprecedented levels. While users marvel at the stunning quality of these synthetic visuals, developers face a growing conundrum: distinguishing these creations from

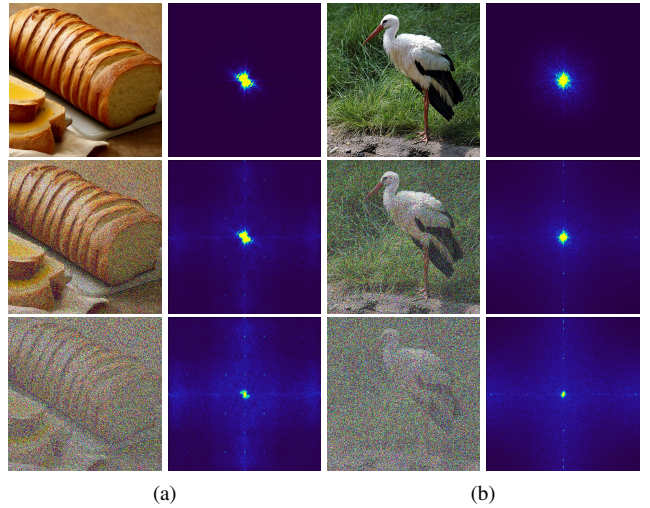


Figure 1. Fourier power spectra of synthetic images (a) and real images (b) at timestep 0 (original), 6, 12 of a 24-timestep DDIM inversion [29] process. Artifacts in the Fourier power spectra of synthesized images manifest as peaks in the high-frequency components of the spectral background, becoming more pronounced with increasing timesteps.

genuine photographs has become increasingly difficult. As the fidelity of generated images continues to improve, the risks and harms of malicious use of these images have also skyrocketed. Can prevailing detection methods keep pace with the sophistication of these knockoffs? Moreover, can current detectors provide explanations robust enough to satisfy skeptics with more than just a feeble “YES”? Existing methods primarily focus on identifying regular images, and human comprehensibility of detection results is yet to be fully explored. This paper seeks to address these gaps, by improving performance on harder detection samples and providing high-quality explanations for synthetic images.

Previous research has explored the properties of deep learning-based generated images from a statistical perspective, focusing on identifying artifacts and fingerprints in the spatial and frequency domains to determine whether an image has been synthesized by deep neural networks such as

^{*}Equal contribution.

[†]Corresponding Author.

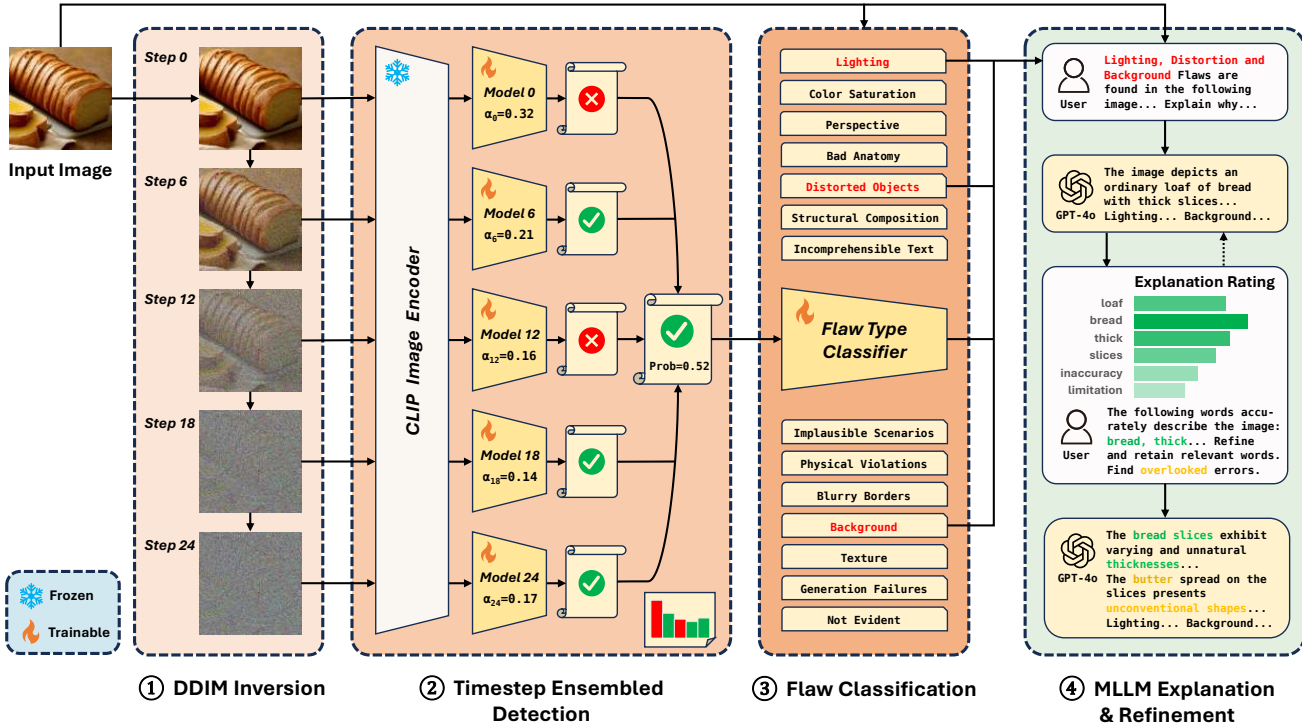


Figure 2. An illustration of the **ESIDE** pipeline. **Stage 1:** The DDIM inversion process progressively adds noise to an input image, creating noised images of various timesteps. **Stage 2:** Synthetic image detection based on AdaBoost ensembling of noised timesteps. **Stage 3:** Multi-label flaw classification to identify the most probable flaws for synthetic images. **Stage 4:** Explanation generation and refinement with MLLMs. Ratings are calculated for the phrases of each explanation and improved throughout refinement iterations.

GANs. More recently, research on diffusion-generated images [20, 36] has further explored their intrinsic characteristics, primarily emphasizing reconstruction-based features by comparing original images with their reconstructed counterparts through diffusion, while overlooking features usable for detection present in images partially-noised for varying timesteps. As shown in Figure 1, we find that synthetic and real images exhibit significant differences in the high-frequency components of their Fourier power spectra, and that diffusion-based noising gradually amplifies these distinctions, providing additional clues for detection.

Salient features useful for discrimination may emerge at different timesteps during the noising process for different images. Based on this observation, we employ an ensemble strategy to aggregate the predictions of multiple classifiers, each trained on images corresponding to a different noised timestep, leading to more robust and accurate detection. Building on this insight, we propose **ESIDE**: Explainable Synthetic Image Detection through Diffusion Timestep Ensembling, a framework designed for detecting diffusion-generated images and synthesizing high-quality explanations, placing particular focus on identifying samples of greater difficulty, as illustrated in Figure 2.

Given an input image of unknown authenticity, our framework first applies DDIM inversion [29] to generate

a series of noised versions of the image across multiple timesteps. These noised versions are subsequently passed through a CLIP [24] image encoder to extract feature representations, which are then fed into an ensemble of models based on AdaBoost [9]. Each model individually predicts whether the image is synthetic, and the final prediction is derived from a weighted sum of the predictions, where the weights are determined by each model’s relative importance. If the image is classified as synthetic, it is further fed into a flaw classification module, which identifies the most probable categories of flaws. A Multimodal Large Language Model (MLLM) is then prompted to generate an explanation based on the identified categories and their descriptions. The explanation is segmented into phrases and iteratively refined according to phrase-image similarity, resulting in a final version of higher quality.

The contributions of this study are three-fold:

- We introduce a novel synthetic image detection method based on ensemble learning of diffusion-noised images. This approach utilizes the additional intrinsic features present in noised images, has a simple architecture, and enables easy distributive training. Experimental results on GenImage [41] show that ESIDE achieves state-of-the-art (SOTA) performance on regular and harder samples, while generalizing effectively on different models.

- We propose an explanation and refinement module capable of generating precise rationales for synthetic images. Phrases of the explanation are rated according to their image similarity, and highly-rated phrases are retained.
- We construct two datasets derived from GenImage: GENHARD and GENEXPLAIN, providing researchers access to harder detection samples and their explanations. The former consists of 108,704 synthetic and 112,682 natural images of greater difficulty, while the latter provides 54,210 groups of AI-generated images paired with their flaws and corresponding explanations.

2. Related Work

2.1. Synthetic Image Detection

Our work focuses on scenarios where only the image itself is provided for detection, without supplementary captions or additional contextual information. Synthetic detection methods by analyzing image characteristics can be broadly categorized into three main approaches [13]: deep learning-based detection, frequency analysis and spatial analysis.

Deep learning-based methods are the most widely adopted. Early detectors primarily targeted images generated by traditional convolutional neural networks (CNNs) [35]. Recently, methods leveraging vision transformers (ViTs) have gained prominence, utilizing CLIP-ViT [24] image encoders for feature extraction, combined with additional modules, linear classifiers or cosine similarity [5, 16, 23, 27, 38]. Other studies focus on identifying discrepancies between synthetic and real images, [20, 36] compared original images with their reconstructions through diffusion, computing reconstruction errors to identify diffusion-generated images. Similarly, Cozzolino *et al.* [6] observed that fake images exhibit a larger gap between actual and expected encoding costs. Tan *et al.* [31] used a pretrained StyleGAN to convert images into gradients, then classified generalized artifacts in them. Nevertheless, the robustness of detection methods for more challenging images remains underexplored, a gap we aim to address in this work.

Frequency analysis methods generally classify synthetic images based on their high-frequency features. Dzanic *et al.* [8] found that generated images share systematic shortcomings in replicating attributes of high-frequency Fourier modes. Corvi *et al.* [4] observed that synthetic images exhibit mid-high frequency signal differences in their spectral power distributions compared to real images. Liu *et al.* [18] utilized frequency inconsistencies among images generated with different models and extracted image frequency domain features. Song *et al.* [30] noted that the frequency domain of diffusion-generated images tends to lean towards a certain direction. Tan *et al.* [32] trained a detector to focus on high-frequency information, exploiting representations across spatial and channel dimensions.

Spatial analysis methods detect fake images by computing pixel-level relations and noise patterns. Liu *et al.* [17] found that the noise patterns of real and synthetic images exhibit distinct characteristics. Zhong *et al.* [40] captured inter-pixel relations and used the contrast between an image’s rich and poor texture regions as its fingerprint. Tan *et al.* [33] employed neighboring pixel relationships, focusing on the local interdependence between image pixels to train an artifact detector. Chen *et al.* [3] proposed a simple method by extracting the simplest patch from the input image and classifying its noise patterns.

2.2. Detection Explainability

Recent studies have explored image forgery explanation using MLLMs [12, 39]. These methods focus on identifying manipulations applied to natural images rather than detecting fully generated images. Li *et al.* [15] introduced a benchmark providing images paired with questions, answers and MLLM-generated explanations. However, this benchmark is limited to 6,000 images, and explanations are manually refined, making it difficult to scale to new image inputs for generating high-quality explanations.

Current explanation frameworks often rely entirely on MLLMs for detection tasks without integrating robust mechanisms. Our work proposes a unified framework combining detection, explanation and automated refinement. When manually filtering our GENEXPLAIN dataset, we found that approximately 67.4% of all the flaws identified by MLLMs (of the SD V1.5 subset) were incorrect. By anchoring the explanation process in the classification results of synthetic errors—rather than relying exclusively on MLLMs—and incorporating a refinement process guided by computable scoring metrics, we effectively mitigate the limitations of MLLMs in standalone detection tasks.

3. Method

3.1. Preliminaries

Diffusion models [1, 21, 26] generate images through a two-stage process involving forward noise addition and reverse denoising. The forward process gradually transforms data into Gaussian noise, while the reverse trains a neural network to iteratively denoise for data distribution restoration. Diffusion models build a symmetric Markov chain that connects the processes, aiming to minimize the KL divergence between the data and noise distributions.

The forward process of the Markov chain is defined as:

$$q(x_t|x_{t-1}) = \mathcal{N}\left(x_t; \sqrt{1 - \beta_t}x_{t-1}, \beta_t\mathbf{I}\right), \quad (1)$$

where x_t represents the noised image at timestep t , and $\beta_t \in (0, 1)$ is a predefined noise schedule.

Denosing Diffusion Probabilistic Models (DDPM) [28] parameterize the reverse process as a Markov chain:

$$p_{\theta}(x_{t-1}|x_t) = \mathcal{N}(x_{t-1}; \mu_{\theta}(x_t, t), \sigma_t^2 \mathbf{I}), \quad (2)$$

where the mean μ_{θ} is derived from a neural network that predicts the noise $\epsilon_{\theta}(x_t, t)$:

$$\mu_{\theta}(x_t, t) = \frac{1}{\sqrt{\alpha_t}} \left(x_t - \frac{\beta_t}{\sqrt{1 - \alpha_t}} \epsilon_{\theta}(x_t, t) \right). \quad (3)$$

Denosing Diffusion Implicit Models (DDIM) [29] accelerate sampling by defining a non-Markovian forward process while maintaining the same marginal distribution $q(x_t|x_0)$. The reverse process combines deterministic generation with stochastic noise injection:

$$x_{t-1} = \sqrt{\bar{\alpha}_{t-1}} \left(\frac{x_t - \sqrt{1 - \bar{\alpha}_t} \epsilon_{\theta}(x_t, t)}{\sqrt{\bar{\alpha}_t}} \right) + \sqrt{1 - \bar{\alpha}_{t-1} - \sigma_t^2} \cdot \epsilon_{\theta}(x_t, t) + \sigma_t \epsilon, \quad (4)$$

3.2. AdaBoost Synthetic Image Detection

In this paper, we propose a novel method for detecting diffusion-generated images through ensemble learning of noised images. AdaBoost (Adaptive Boosting), originally proposed by Freund and Schapire [9], is a boosting algorithm designed to improve the performance of classification tasks. By ensembling multiple weak models and aggregating their predictions through a weighted sum, AdaBoost constructs a stronger learner with enhanced accuracy.

Specifically, for the task of synthetic image detection, given an input image x_0 , we apply a T -timestep DDIM inversion process to yield intermediate noise samples, generating a sequence of stepwise noised images: $\{x_0, x_1, x_2, \dots, x_T\}$. For each timestep divisible by a stride s , a base classifier m_k (where $k = 0, s, 2s, \dots, T$ and $T \bmod s \equiv 0$) is trained exclusively on the corresponding noised images, resulting in a collection of models M :

$$M = \{m_0, m_s, m_{2s}, \dots, m_T\} \quad (5)$$

A **sample weight** $w_{k,i}$ is assigned to each image of the training set to emphasize samples previously misclassified, while reducing the significance of correctly predicted cases. As each model operates on a noised dataset corresponding to a different diffusion timestep, the sample weights are initialized individually for each model, where N represents the total number of images in the training set.

$$w_{k,1} = w_{k,2} = \dots = w_{k,n} = \frac{1}{N} \quad (6)$$

The sample weights $w_{k,i}$ are incorporated into the binary cross-entropy (BCE) loss function, yielding a weighted loss

function $\mathcal{L}_{\text{WBCE}}$, where y denotes the true label and \hat{y} is the predicted probability:

$$\mathcal{L}_{\text{WBCE}}(k, y, \hat{y}) = \sum_{i=1}^N w_{k,i} [y_i \log(\hat{y}_i) + (1 - y_i) \log(1 - \hat{y}_i)] \quad (7)$$

The weighted error ϵ_k of m_k can then be calculated as:

$$\epsilon_k = \frac{\sum_{i=1, h_k(x_i) \neq y_i}^N w_{k,i}}{\sum_{i=1}^N w_{k,i}} \quad (8)$$

where $h_k(x_i)$ is the prediction of m_k for sample x_i .

To form the final prediction, a **model weight** α_k is assigned to each classifier and updated throughout training:

$$\alpha_k = \frac{1}{2} \ln \left(\frac{1 - \epsilon_k}{\epsilon_k} \right) \quad (9)$$

Sample weights are then adjusted according to the prediction results and normalized:

$$\tilde{w}_{k,i} = w_{k,i} \cdot e^{-\eta \alpha_k \cdot h_k(x_i) y_i} \quad (10)$$

$$w'_{k,i} = \frac{\tilde{w}_{k,i}}{\sum_{i=1}^N \tilde{w}_{k,i}} \quad (11)$$

where η is a learning rate factor applied to limit change rate.

Finally, after training the base classifiers, model weights α_k are used to calculate a weighted sum $H(x_i)$ of the predictions from each m_k for the final prediction of image x_i :

$$H(x_i) = \text{sign} \left(\sum_{k=0}^T \alpha_k \cdot h_k(x_i) \right) \quad (12)$$

In practice, a threshold is applied to the weighted error to normalize model weights and prevent degradation.

3.3. Explanation Refinement

To investigate the rationale behind synthetic images, we employ a simple multi-label classifier to identify potential flaws present in the image. MLLMs are utilized to generate a rough explanation for each image based on the identified types. An iterative refinement process is then conducted to enhance explanation quality, where the initial explanation is segmented into multiple phrases, and each phrase is assigned a rating based on its semantic similarity to the image.

We leverage text-image cross attention [14] mechanisms to compute these ratings. Faster R-CNN [25] is first applied to the image for object detection, identifying n sub-image regions. These regions are then encoded into embeddings v_1, v_2, \dots, v_n using a CLIP Vision Transformer (ViT). The embedding of the full image v_0 is also included in the list of region embeddings. The phrase e is then encoded into the same vector space, and its similarity with each region is calculated and normalized as follows:

	LI	CS	PS	BA	DO	SC	IT	IS	PV	BB	BG	TX	GF	NE	#	
Midjourney																4,561
SD V1.4																7,712
SD V1.5																4,556
ADM																6,932
GLIDE																7,681
Wukong																7,488
VQDM																7,822
BigGAN																7,458
#	3,324	510	2,161	13,902	13,651	4,232	4,568	439	1,295	2,811	960	1,908	461	3988	54,210	

Flaws: Lighting, Distorted Objects, Background

- The slices lack standard uniformity, exhibiting varying and unnatural thicknesses that undermine the appearance of a properly sliced loaf. The butter spread on the slices presents unconventional shapes and inconsistent textures. ...
- The top crust of the bread is overly bright, suggesting the presence of multiple conflicting light sources rather than a singular direction. The upper layer of butter appears excessively illuminated while the lower slice casts an unrealistic shadow, lacking alignment with any visible light source. ...
- The background suffers from poorly blended monotonous drabness, dominated by unvarying brown tones of the wooden surface. ...

Figure 3. Visualization of the **GenExplain** Dataset. Synthetic images from GenImage are divided into 14 categories of flaws. Abbreviation is employed for convenience of display. **LI**: Lighting, **CS**: Color Saturation or Contrast, **PS**: Perspective, **BA**: Bad Anatomy, **DO**: Distorted Objects, **SC**: Structural Composition, **IT**: Incomprehensible Text, **IS**: Implausible Scenarios, **PV**: Physical Law Violations, **BB**: Blurry or Inconsistent Borders, **BG**: Background, **TX**: Texture, **GF**: Generation Failures, **NE**: Not Evident. The total number of images is displayed in the last row and column. Each image is matched with one or more categories, with a corresponding explanation for each flaw type.

$$\tilde{s}_i = \frac{\cos\langle e, v_i \rangle}{\sum_{i=0}^n \cos\langle e, v_i \rangle} \quad (13)$$

A weighted combination of the region embeddings, denoted as a , is derived based on the similarities:

$$a = \sum_{i=0}^n \frac{v_i \cdot e^{\lambda \tilde{s}_i}}{\sum_{i=0}^n e^{\lambda \tilde{s}_i}} \quad (14)$$

where λ denotes the inverse temperature of the softmax function. The **rating** of the phrase is then calculated as its cosine similarity with a .

For refinement, the MLLM is instructed to retain phrases with high relevance while identifying additional flawed regions that may have been overlooked. This process is iteratively repeated with the revised explanations for a number of rounds, resulting in a final explanation that describes the flaws present in the image with greater accuracy.

3.4. Construction of GenHard and GenExplain

We constructed two novel datasets, **GENHARD** and **GENEXPLAIN**, based on GenImage [41]. The former comprises synthetic and natural images more challenging to detect, while the latter aims to categorize and provide explanations for flaws commonly found in artificial images.

GenHard To extract samples of greater difficulty, we employed the CBSID [5] baseline detector with a Net-XS classifier (described in Section 4.3). Classifiers were trained for a single epoch on a partition of the validation subsets of GenImage, and subsequently tested on each training subset. Across the 8 subsets, the 108,704 synthetic images and 112,682 natural images misclassified were identified as hard samples. These samples were then partitioned into training and validation sets by a ratio of approximately 9:1.

GenExplain We identified 14 common categories of flaws associated with realistic synthetic images [15, 39], and constructed a dataset comprising 54,210 groups of images, flaws and explanations, illustrated in Figure 3. Images from each validation subset of GenImage were fed into gpt-4o, along with a prompt with the definition of the flaws and instructions. This step yielded a preliminary categorization of approximately 11,000 to 14,000 image-flaw pairs per subset. We then manually removed 30.1% to 67.4% of the images that were baselessly categorized from each subset, which also indicates that current MLLMs may not perform ideally at classifying image errors. Subsequently, gpt-4o was prompted to generate explanations for the pairs remaining. After a rating and refinement process to ensure precision, the final explanations are obtained.

Method	Training & Test Subsets								Avg. Acc (%)
	Midjourney	SD V1.4	SD V1.5	ADM	GLIDE	Wukong	VQDM	BigGAN	
ResNet-50 [11]	83.90/86.75	80.63/94.17	76.17/90.19	75.81/91.00	95.82 /99.00	73.72/89.50	92.94/98.67	99.10 /96.08	84.76/93.17
DeiT-S [34]	58.29/76.08	73.92/81.08	74.32/78.75	63.37/68.42	72.84/93.83	71.01/83.83	66.87/77.50	46.23/76.00	65.86/79.44
Swin-T [19]	70.81/91.00	74.63/88.08	78.02/90.00	70.30/79.50	85.19/97.83	74.92/85.92	86.96/90.17	88.24/ <u>99.67</u>	78.63/90.27
CNNSpot [35]	70.91/83.92	78.02/89.25	80.15/88.06	68.32/72.58	78.57/87.08	78.95/87.83	89.97/97.42	70.44/96.08	76.92/87.78
CBSID [5]	67.10/93.25	73.03/90.92	72.22/93.63	94.20/99.83	88.53/99.17	75.67/92.75	84.10/98.17	98.27/ 99.91	81.64/95.95
DIRE [36]	<u>88.86</u> /92.83	<u>95.72</u> / <u>97.42</u>	96.02/96.25	90.52/94.67	81.40/ 99.83	84.17/92.67	94.90/97.83	93.29/ <u>99.67</u>	90.91/96.40
LGrad [31]	72.25/87.33	72.28/83.92	76.45/84.37	70.86/79.17	82.19/96.00	65.50/79.75	74.80/81.08	83.74/94.58	74.76/85.78
UnivFD [23]	40.80/87.75	41.92/89.33	35.40/88.25	65.28/85.58	79.13/94.25	65.35/89.42	67.84/91.92	71.07/94.75	58.35/90.16
FreqNet [32]	87.13/94.33	93.47/94.58	96.73 /95.12	95.69/91.50	82.13/98.25	90.88/90.17	98.60 /95.42	85.12/99.17	91.22/94.82
NPR [33]	85.10/87.25	89.90/95.25	<u>95.23</u> / <u>97.12</u>	<u>99.36</u> / <u>99.75</u>	<u>86.29</u> / <u>92.08</u>	96.94 / 98.42	93.74/97.33	92.87/99.58	<u>92.43</u> / <u>95.85</u>
ESIDE-M (ours)	83.14/ <u>95.67</u>	89.73/96.75	89.68/97.06	<u>99.22</u> / <u>99.92</u>	<u>94.42</u> / <u>99.33</u>	87.30/94.67	97.27/ 99.50	99.10 /99.33	<u>92.48</u> / <u>97.78</u>
ESIDE-L (ours)	92.38 / 98.42	96.65 / 99.17	96.73 / 98.63	99.43 / 100.00	<u>94.98</u> / <u>99.00</u>	<u>91.50</u> / <u>97.25</u>	<u>97.90</u> / <u>99.33</u>	97.58/99.50	95.89 / 98.91

Table 1. Synthetic image detection accuracy on GenImage subsets. Models are trained individually on each GenImage subset, with the **original** samples training set only, while tested on both the **original** samples test set, and a previously unseen **hard** samples test set from GenHard. The prior number for each cell marks the test accuracy on the **hard** samples, while the posterior marks the test accuracy on the **original** samples. The best scores are highlighted in **bold**, and the second best are underlined.

4. Experiments

4.1. Synthetic Image Detection

We train an AdaBoost ensemble on groups of noised images derived from DDIM inversion intermediate timesteps, following the diffusion implementation provided by [36] and using pre-trained diffusion models of sizes 256×256 and 512×512 from [7]. A CLIP ViT-L/14 [24] image encoder is first employed to extract image features, which are then passed through a simple linear network for binary classification, following a procedure similar to that proposed in [5]. After each ensemble model generates a prediction, the final prediction is obtained by computing a weighted sum of their predicted labels based on their model weights α_k .

GenImage GenImage [41] is a million-scale dataset consisting of 1,331,167 real images and 1,350,000 generated images, distributed across 8 generator subsets: Midjourney [21], Stable Diffusion V1.4 [26], Stable Diffusion V1.5 [26], ADM [7], GLIDE [22], Wukong [37], VQDM [10], and BigGAN [2].

Following the settings of GenImage, we evaluate and compare our method with baselines on both the original GenImage dataset and the more challenging samples curated in GENHARD. Two distinct scenarios are investigated for training and evaluation: (1) train-test subsets from the same generator, and (2) train-test subsets sourced from different generators, enabling a comprehensive assessment of robustness and generalization.

Implementation Details A total of $T = 24$ DDIM inversion timesteps are taken to generate the noised images. The sample weights learning rate η is set to 0.25, and clas-

sifier error thresholds $\epsilon_k = \min(\max(\tilde{\epsilon}_k, 0.001), 0.5)$ are enforced to prevent model weight overflow and ensemble degradation. Due to computational resource constraints, we partition the validation subsets of GenImage in a 9:1 ratio for training and evaluation.

We primarily evaluate our method on two architectures: Net-M and Net-L (detailed differences are provided in Section 4.3). ESIDE-M is a lightweight ensemble of 4 models, with a stride $s = 8$ and a smaller network. ESIDE-L is a more performance-oriented ensemble of 9 models, with a stride $s = 3$ and a larger network. A batch normalization layer, a LeakyReLU activation with a negative slope of 0.1, and a Dropout layer with a dropout rate of 0.5 are sequentially applied after each linear layer. The AdamW optimizer with a learning rate of 1×10^{-4} and weight decay of 5×10^{-4} is employed, alongside our modified weighted binary cross-entropy loss function $\mathcal{L}_{\text{WBCE}}$. Our implementation is built on the PyTorch framework, with computational support provided by NVIDIA L20 48GB GPUs. Due to the simplicity of the network architecture of our classifier, our method exhibits low GPU memory consumption, and can complete training rapidly if the CLIP features of the images are precomputed and stored.

Result Analysis As shown in Table 1, our ESIDE-L model achieves SOTA performance on both harder samples and the original images, with an average absolute accuracy increase of at least 3.46% and 2.51%, respectively. ESIDE-L performs 16.04% better than baseline averages on harder samples and leads by 7.95% on originals. Cross-validation results in Table 2 show that our method also generalizes effectively across subsets of images synthesized by other diffusion models.

Method	Test Subsets								Avg. Acc (%)
	Midjourney	SD V1.4	SD V1.5	ADM	GLIDE	Wukong	VQDM	BigGAN	
ResNet-50 [11]	51.54/61.33	77.67/93.75	76.17/90.19	67.26/49.58	26.02/50.50	75.56/88.17	46.14/50.75	26.99/47.75	55.92/66.50
DeiT-S [34]	46.69/50.42	73.14/80.08	74.32/78.75	64.64/46.50	26.11/46.92	73.33/78.00	46.66/46.33	29.97/44.42	54.36/58.93
Swin-T [19]	50.62/62.58	77.70/90.67	78.02/90.00	60.75/50.75	25.46/53.83	76.39/86.25	42.12/50.42	25.88/49.17	54.62/66.71
CNNSpot [35]	49.40/54.50	78.24/87.92	80.15/88.06	71.78/48.00	25.52/53.33	75.82/81.75	49.63/50.75	28.65/48.67	57.40/64.12
CBSID [5]	50.55/76.42	70.07/91.33	72.22/93.63	73.97/54.50	38.91/68.92	70.27/74.75	51.63/63.67	32.46/54.50	57.51/72.22
DIRE [36]	68.06/63.25	95.75/96.67	96.02/96.25	35.08/36.58	32.10/16.17	59.42/55.50	37.50/30.17	43.11/19.08	58.38/51.71
LGrad [31]	54.07/59.25	75.42/83.08	76.45/84.37	77.65/49.42	25.70/51.08	59.42/61.58	51.69/49.08	29.48/49.08	56.24/60.87
UnivFD [23]	31.43/80.50	37.50/90.42	35.40/88.25	69.52/53.00	31.62/70.67	52.40/76.08	47.89/57.08	31.14/58.83	42.11/71.85
FreqNet [32]	74.89/72.50	95.58/96.67	96.73/95.12	75.46/54.42	45.27/65.00	87.52/77.08	52.99/54.42	73.56/77.17	75.25/74.05
NPR [33]	52.93/53.17	95.72/97.67	95.23/97.12	71.36/55.50	54.39/70.42	91.34/95.08	50.79/50.42	31.90/50.25	67.96/71.20
ESIDE-M (ours)	60.45/74.83	88.73/96.67	89.68/97.06	68.11/43.25	49.73/56.50	81.99/75.67	64.77/59.50	49.62/61.67	69.14/70.64
ESIDE-L (ours)	61.49/71.25	95.51/99.34	96.73/98.63	60.18/33.00	60.88/47.25	81.64/68.08	68.51/58.00	83.18/61.67	76.02/67.15

Table 2. Cross-validation accuracy on GenImage subsets. Models are trained on GenImage/SD V1.5 with the **original** samples training set only, while tested on another subset on both the **original** samples test set, and a previously unseen **hard** samples test set from GenHard.

Settings		Midjourney	SD V1.4	SD V1.5	ADM	GLIDE	Wukong	VQDM	BigGAN	Avg.
Net-M	EM	39.94	52.40	56.82	48.98	48.81	34.85	47.41	49.07	47.29
	mAP	32.83	35.54	33.76	39.59	35.85	34.20	47.78	33.69	36.66
Net-L	EM	41.60	52.03	58.08	50.41	49.72	33.81	54.61	49.07	48.67
	mAP	34.70	35.71	33.01	40.04	34.57	33.80	54.05	34.50	37.55

Table 3. Performance of 14-type flaw classification on GenExplain subsets.

Notably, some methods perform worse than random guessing on hard samples. This is reasonable, as only incorrectly identified images are included in GENHARD, further underscoring its difficulty. Similar cross-validation results reveal that effective indicators for one diffusion model may perform just the opposite on another, highlighting the challenges in generalizing detection methods.

4.2. Error Explanation

Flaw Classification We propose a simple baseline and conduct experiments on GENEXPLAIN to classify synthetic flaws. The same model architectures as that in Section 4.1 are adopted, with the size of the output layer adjusted to 14 to match the categories of flaw types, and BCE Loss is used. A predicted label is considered “True” if the model’s output logit is greater than or equal to 0.5 and “False” otherwise. The predictions for each flaw label are computed independently. We partition our dataset by 9:1 for training and eval-

uation. Evaluation metrics include Exact Match (EM) accuracy and Mean Average Precision (mAP). EM measures the proportion of predictions where all 14 labels are correctly matched, while mAP calculates the mean value of the Average Precision (AP) across all labels.

Results are presented in Table 3. The classifier trained on Net-L generally outperforms its counterpart trained on Net-M. However, both models exhibit inferior performance on Midjourney and Wukong compared to other subsets.

Explanation Refinement Following the methodology outlined in Section 3.3, we instruct `gpt-4o` to generate the initial and refined explanations. We iteratively rewrite the explanations over 3 iterations and assess the quality of each version. To objectively measure the association between synthetic images and explanations, we adopt Top-5, Top-10, and Overall Similarity between text phrases and image regions as evaluation metrics, which guide the refinement process. Figure 4 illustrates an example of how this similarity is assessed. We instruct `gpt-4o` to retain the top 10 phrases during each iteration. Additionally, we employ three natural language metrics: Type-Token-Ratio (TTR \uparrow), Perplexity (PPL \downarrow) and normalized Shannon Entropy (SE \uparrow), to evaluate informativeness and diversity. TTR and SE are computed based on the entire set of explanations, while PPL is obtained using `gpt-2`. These metrics reflect lexical diversity, information density and fluency, respectively.

The AI-generated image exhibits the **systematic error** of **distorted objects**, particularly evident in the **sliced bread** and the **battered portions**. The **slices** of **bread** show an **unnatural curvature** and **uneven thickness**, deviating from the **expected straight cuts** found in **typical loaves**. Additionally, the **butter** appears to be **inconsistently spread**, with some **areas** looking excessively thick and others almost non-existent, leading to an unrealistic presentation. These **anomalies** create an **illusion of warped forms**, which detracts from the recognizable and expected features of **unprocessed bread** and **butter**.

$$\text{sim}_5 = \frac{(\text{bread} + \text{sliced_bread} + \text{unprocessed_bread} + \text{butter} + \text{typical_loaves})/5}{0.235} = 0.235$$

Figure 4. Illustration of the similarities of noun phrases with the image in an explanation snippet, and calculation of Top-5 average.

Metric	Original	Refined-v1	Refined-v2	Refined-v3
\overline{sim}_5 (\uparrow)	0.2217	0.2239	0.2253	0.2261
\overline{sim}_{10} (\uparrow)	0.2050	0.2074	0.2089	0.2099
\overline{sim} (\uparrow)	0.1845	0.1858	0.1865	0.1870
TTR (\uparrow)	0.01951	0.01990	0.01992	0.01995
SE (\uparrow)	0.4637	0.4684	0.4701	0.4712
PPL (\downarrow)	40.32	43.55	44.84	45.58

Table 4. Evaluation metrics of each iteration during the explanation refinement process on GenExplain/SD V1.5.

Results are shown in Table 4 and Figure 5. Throughout refinement iterations, monotonic increases in similarity, TTR and SE indicate that refined explanations have higher relevance with the original image, and possess higher lexical and information density. However, increases in PPL indicate that refined versions have less fluency, which may be attributed to the retention of specialized or domain-specific terms uncommon in general language usage.

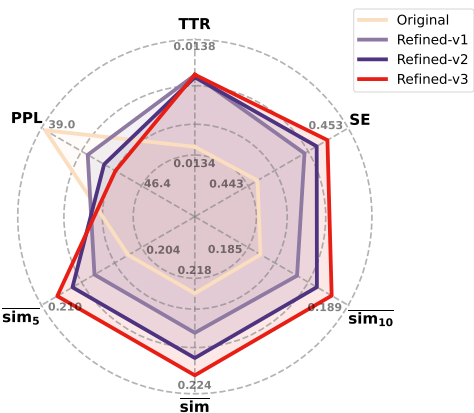


Figure 5. Metrics average across all 8 subsets of GenExplain regarding the initial explanations and their refined versions.

4.3. Ablation Studies

Model Architecture RQ1: How is the architecture of the linear classifier chosen, and does ensembling multiple models yield better performance than a single Step-0 detector?

The performance of the CBSID baseline [5], trained on noised images from various timesteps, is presented in Table 5. Sharing a similar classifier architecture as ours, the model trained solely on Step-0 images significantly outperforms those trained on other timesteps. Does this imply that

Timestep	0	3	6	9	12	15	18	21	24
Acc	99.25	93.42	93.00	93.33	94.48	96.17	96.50	96.75	96.42

Table 5. Performance of 9 CBSID classification models on original samples, individually trained on noised images from different diffusion timesteps. Models are trained on GenImage/GLIDE, Net-XS architecture, with stride s set to 3.

detectors trained on Step-3 to Step-24 for our ensemble are unnecessary? To answer this question, we evaluated various architectures. Each network has an input size of 768 and an output size of 1, with hidden layer sizes as listed below:

- **Net-XS:** 256
- **Net-S:** 512, 256
- **Net-M:** 512, 256, 128
- **Net-L:** 1024, 512, 256, 128
- **Net-XL:** 1024, 1024, 512, 256, 128
- **Net-LW:** 2048, 1024, 512, 256

As shown in Table 6, the “ESIDE w/o α_k ” setting retains only α_0 and sets the **model weights** of all other timesteps to 0, i.e., only training a single model on original images, while CBSID is equivalent to additionally deactivating our **sample weights** training strategy. Under either circumstance, performance is significantly reduced.

Architecture	ESIDE	ESIDE w/o α_k	CBSID [5]
Net-XS	89.79/98.75	78.27/96.92	74.03/99.25
Net-S	92.22/98.67	89.44/99.00	86.86/ 99.33
Net-M	94.42/ 99.33	88.92/99.25	87.93/99.08
Net-L	94.98 /99.00	88.75/98.92	88.53/99.17
Net-XL	93.56/98.42	89.59/98.67	86.92/99.25
Net-LW	93.34/98.50	86.83/98.42	86.12/ 99.33

Table 6. Comparison of effects of model architectures on detection results. Models are trained on GenImage/GLIDE, with stride s set to 3. “ESIDE w/o α_k ” retains only α_0 , while “CBSID” additionally compares not using our sample weights training strategy.

Unnoised Images RQ2: Is ensembling models on noised images from different timesteps necessary? Would training the ensemble on unnoised images do better?

To test this hypothesis, we trained the “AdaBoost-Original” setting completely on the original images dataset. Table 7 demonstrates that our method achieves an absolute accuracy increase of 5.7% on hard samples compared to ensembling entirely on unnoised images. “AdaBoost-Original” shows no evident difference from the single-model classifier CBSID in Table 1, which we conjecture may be due to the loss of intrinsic characteristics resulting from the exclusion of noised images, as well as the overly consistent performance of the models and similar α_k values.

Architecture	ESIDE	AdaBoost-Original	Δ
Net-M	94.42/99.33	88.62/99.25	5.80 /0.08
Net-L	94.98/99.00	89.27/99.00	5.71 /0.00

Table 7. Comparison of ESIDE detection results with training an ensemble completely on unnoised images, each model initialized with a different seed. Models are trained on GenImage/GLIDE, with stride s set to 8 for Net-M and set to 3 for Net-L.

Diffusion Timestep Stride RQ3: What impact does the number of models in the ensemble have on performance?

Different model architectures exhibit preferences for different strides, i.e., ensemble sizes, as depicted in Table 8. ESIDE-M, which attains optimal performance at a stride size of 8, is the most training-efficient. Notably, performance remains constant when Net-XS adopts a stride of $s = 6, 8, 12$. This occurs because under these settings, the trained model weights $\alpha_0 > \sum_{k=s}^T \alpha_k$, resulting in the degradation of the ensembles to a single Step-0 model.

Stride Size	ESIDE-XS	ESIDE-M	ESIDE-L
$s = 1$	91.10 /97.75	92.99/99.00	93.30/98.58
$s = 2$	90.71/98.58	92.65/98.92	93.53/98.42
$s = 3$	89.33/98.83	93.02/98.75	94.98/99.00
$s = 4$	87.86/ 99.25	92.97/98.75	93.21/98.33
$s = 6$	83.90/97.75	92.69/99.00	92.95/98.33
$s = 8$	83.90/97.75	94.42/99.33	93.94/98.75
$s = 12$	83.90/97.75	94.12/98.67	91.77/98.42

Table 8. Comparison of different stride size on detection results. Models are trained on GenImage/GLIDE, with model architectures Net-XS, Net-M and Net-L tested.

5. Conclusion

In this paper, we present ESIDE, a novel framework for detecting and explaining synthetic images. We explore the distinct high-frequency features between synthetic and real images noised through DDIM-inversion and train an ensemble on noised images to enhance detection performance. To improve human perception of fake images, we introduce an explanation generation and refinement module. Additionally, we construct two datasets, GENHARD and GENEXPLAIN, comprising more challenging samples and providing categorized flaw types with explanations for AI-generated images, respectively. Extensive experiments show that ESIDE achieves SOTA performance on both regular and harder images, with significant improvements on samples of greater difficulty. Our method also generalizes effectively across synthetic images generated by other diffusion models.

Limitations

Ensembling is a strategy that trades efficiency for performance. As our detection method utilizes partially noised images, a preceding time-consuming DDIM inversion process is required. While our simple network architecture enables each model to consume less training time than existing detectors, the need to train multiple models cannot be denied. Time consumption could be alleviated by precomputing and storing the CLIP features of images, or employing distributed parallel training followed by fusing the models

into an ensemble. Additionally, since we rely on MLLMs for explanation refinement, the quality of the explanations remains dependent on MLLM performance. Though average quality metrics improved throughout the refinement of GENEXPLAIN, there remain inevitable rare cases where the model underperforms and generates lower-rated explanations, leading to a loss of refinement effectiveness.

Societal Impacts

Advances in diffusion models and AI-generated content have enabled the creation of deceptively real images, delighting users while simultaneously raising significant ethical concerns. Our study offers a novel solution to the rapidly evolving landscape of synthetic image detection, aiming to address the societal challenges posed by the malicious use of AI-generated images and hopes to mitigate potential security risks associated with their proliferation. We employ GPT-4o to generate explanations for synthetic images, which may occasionally produce uncontrollable generated content requiring further discrimination. Another point to note is that our GENHARD and GENEXPLAIN datasets use images from the GenImage benchmark, which may include disturbing malformed images generated by diffusion models, particularly those regarding humans or animals.

References

- [1] James Betker, Gabriel Goh, Li Jing, Tim Brooks, Jianfeng Wang, Linjie Li, Long Ouyang, Juntang Zhuang, Joyce Lee, Yufei Guo, et al. Improving image generation with better captions. *Computer Science*. <https://cdn.openai.com/papers/dall-e-3.pdf>, 2(3):8, 2023. 1, 3
- [2] Andrew Brock, Jeff Donahue, and Karen Simonyan. Large scale gan training for high fidelity natural image synthesis. In *International Conference on Learning Representations*, 2019. 6
- [3] Jiaxuan Chen, Jieteng Yao, and Li Niu. A single simple patch is all you need for ai-generated image detection. *arXiv preprint arXiv:2402.01123*, 2024. 3
- [4] Riccardo Corvi, Davide Cozzolino, Giovanni Poggi, Koki Nagano, and Luisa Verdoliva. Intriguing properties of synthetic images: from generative adversarial networks to diffusion models. In *Proceedings of the IEEE/CVF conference on computer vision and pattern recognition*, pages 973–982, 2023. 3
- [5] Davide Cozzolino, Giovanni Poggi, Riccardo Corvi, Matthias Nießner, and Luisa Verdoliva. Raising the bar of ai-generated image detection with clip. In *Proceedings of the IEEE/CVF Conference on Computer Vision and Pattern Recognition*, pages 4356–4366, 2024. 3, 5, 6, 7, 8
- [6] Davide Cozzolino, Giovanni Poggi, Matthias Nießner, and Luisa Verdoliva. Zero-shot detection of ai-generated images. In *European Conference on Computer Vision*, pages 54–72. Springer, 2024. 3

- [7] Prafulla Dhariwal and Alexander Nichol. Diffusion models beat gans on image synthesis. *Advances in neural information processing systems*, 34:8780–8794, 2021. 6
- [8] Tarik Dzanic, Karan Shah, and Freddie Witherden. Fourier spectrum discrepancies in deep network generated images. *Advances in neural information processing systems*, 33:3022–3032, 2020. 3
- [9] Yoav Freund and Robert E Schapire. A decision-theoretic generalization of on-line learning and an application to boosting. *Journal of computer and system sciences*, 55(1):119–139, 1997. 2, 4
- [10] Shuyang Gu, Dong Chen, Jianmin Bao, Fang Wen, Bo Zhang, Dongdong Chen, Lu Yuan, and Baining Guo. Vector quantized diffusion model for text-to-image synthesis. *2022 IEEE/CVF Conference on Computer Vision and Pattern Recognition (CVPR)*, pages 10686–10696, 2021. 6
- [11] Kaiming He, X. Zhang, Shaoqing Ren, and Jian Sun. Deep residual learning for image recognition. *2016 IEEE Conference on Computer Vision and Pattern Recognition (CVPR)*, pages 770–778, 2015. 6, 7
- [12] Zhengchao Huang, Bin Xia, Zicheng Lin, Zhun Mou, Wenming Yang, and Jiaya Jia. Ffaa: Multimodal large language model based explainable open-world face forgery analysis assistant. *arXiv preprint arXiv:2408.10072*, 2024. 3
- [13] Linda Laurier, Ave Giuletta, Arlo Octavia, and Meade Cleti. The cat and mouse game: The ongoing arms race between diffusion models and detection methods. *arXiv preprint arXiv:2410.18866*, 2024. 3
- [14] Kuang-Huei Lee, Xi Chen, Gang Hua, Houdong Hu, and Xiaodong He. Stacked cross attention for image-text matching. In *Proceedings of the European conference on computer vision (ECCV)*, pages 201–216, 2018. 4
- [15] Yixuan Li, Xuelin Liu, Xiaoyang Wang, Bu Sung Lee, Shiqi Wang, Anderson Rocha, and Weisi Lin. Fakebench: Probing explainable fake image detection via large multimodal models. *arXiv preprint arXiv:2404.13306*, 2024. 3, 5
- [16] Li Lin, Irene Amerini, Xin Wang, Shu Hu, et al. Robust clip-based detector for exposing diffusion model-generated images. In *2024 IEEE International Conference on Advanced Video and Signal Based Surveillance (AVSS)*, pages 1–7. IEEE, 2024. 3
- [17] Bo Liu, Fan Yang, Xiuli Bi, Bin Xiao, Weisheng Li, and Xinbo Gao. Detecting generated images by real images. In *European Conference on Computer Vision*, pages 95–110. Springer, 2022. 3
- [18] Yang Liu, Xiaofei Li, Jun Zhang, Shengze Hu, and Jun Lei. Da-hfnet: Progressive fine-grained forgery image detection and localization based on dual attention. In *2024 3rd International Conference on Image Processing and Media Computing (ICIPMC)*, pages 51–58. IEEE, 2024. 3
- [19] Ze Liu, Yutong Lin, Yue Cao, Han Hu, Yixuan Wei, Zheng Zhang, Stephen Lin, and Baining Guo. Swin transformer: Hierarchical vision transformer using shifted windows. *2021 IEEE/CVF International Conference on Computer Vision (ICCV)*, pages 9992–10002, 2021. 6, 7
- [20] Yunpeng Luo, Junlong Du, Ke Yan, and Shouhong Ding. Lare²: Latent reconstruction error based method for diffusion-generated image detection. In *Proceedings of the IEEE/CVF Conference on Computer Vision and Pattern Recognition*, pages 17006–17015, 2024. 2, 3
- [21] Midjourney, 2022. <https://www.midjourney.com/home/>. 1, 3, 6
- [22] Alex Nichol, Prafulla Dhariwal, Aditya Ramesh, Pranav Shyam, Pamela Mishkin, Bob McGrew, Ilya Sutskever, and Mark Chen. Glide: Towards photorealistic image generation and editing with text-guided diffusion models. In *International Conference on Machine Learning*, 2021. 6
- [23] Utkarsh Ojha, Yuheng Li, and Yong Jae Lee. Towards universal fake image detectors that generalize across generative models. In *Proceedings of the IEEE/CVF Conference on Computer Vision and Pattern Recognition*, pages 24480–24489, 2023. 3, 6, 7
- [24] Alec Radford, Jong Wook Kim, Chris Hallacy, Aditya Ramesh, Gabriel Goh, Sandhini Agarwal, Girish Sastry, Amanda Askell, Pamela Mishkin, Jack Clark, Gretchen Krueger, and Ilya Sutskever. Learning transferable visual models from natural language supervision. In *International Conference on Machine Learning*, 2021. 2, 3, 6
- [25] Shaoqing Ren, Kaiming He, Ross Girshick, and Jian Sun. Faster r-cnn: Towards real-time object detection with region proposal networks. *Advances in neural information processing systems*, 28, 2015. 4
- [26] Robin Rombach, A. Blattmann, Dominik Lorenz, Patrick Esser, and Björn Ommer. High-resolution image synthesis with latent diffusion models. *2022 IEEE/CVF Conference on Computer Vision and Pattern Recognition (CVPR)*, pages 10674–10685, 2021. 1, 3, 6
- [27] Zeyang Sha, Zheng Li, Ning Yu, and Yang Zhang. De-fake: Detection and attribution of fake images generated by text-to-image generation models. In *Proceedings of the 2023 ACM SIGSAC conference on computer and communications security*, pages 3418–3432, 2023. 3
- [28] Jascha Sohl-Dickstein, Eric Weiss, Niru Maheswaranathan, and Surya Ganguli. Deep unsupervised learning using nonequilibrium thermodynamics. In *International conference on machine learning*, pages 2256–2265. pmlr, 2015. 4
- [29] Jiaming Song, Chenlin Meng, and Stefano Ermon. Denoising diffusion implicit models. In *International Conference on Learning Representations*, 2021. 1, 2, 4
- [30] Jiawei Song, Dengpan Ye, and Yunming Zhang. Trinity detector: text-assisted and attention mechanisms based spectral fusion for diffusion generation image detection. *IEEE Signal Processing Letters*, 2024. 3
- [31] Chuangchuang Tan, Yao Zhao, Shikui Wei, Guanghua Gu, and Yunchao Wei. Learning on gradients: Generalized artifacts representation for gan-generated images detection. In *Proceedings of the IEEE/CVF Conference on Computer Vision and Pattern Recognition*, pages 12105–12114, 2023. 3, 6, 7
- [32] Chuangchuang Tan, Yao Zhao, Shikui Wei, Guanghua Gu, Ping Liu, and Yunchao Wei. Frequency-aware deepfake detection: Improving generalizability through frequency space domain learning. In *Proceedings of the AAAI Conference on Artificial Intelligence*, pages 5052–5060, 2024. 3, 6, 7

- [33] Chuangchuang Tan, Yao Zhao, Shikui Wei, Guanghua Gu, Ping Liu, and Yunchao Wei. Rethinking the up-sampling operations in cnn-based generative network for generalizable deepfake detection. In *Proceedings of the IEEE/CVF Conference on Computer Vision and Pattern Recognition*, pages 28130–28139, 2024. 3, 6, 7
- [34] Hugo Touvron, Matthieu Cord, Matthijs Douze, Francisco Massa, Alexandre Sablayrolles, and Hervé Jégou. Training data-efficient image transformers & distillation through attention. In *International Conference on Machine Learning*, 2020. 6, 7
- [35] Sheng-Yu Wang, Oliver Wang, Richard Zhang, Andrew Owens, and Alexei A. Efros. Cnn-generated images are surprisingly easy to spot... for now. *2020 IEEE/CVF Conference on Computer Vision and Pattern Recognition (CVPR)*, pages 8692–8701, 2019. 3, 6, 7
- [36] Zhendong Wang, Jianmin Bao, Wen gang Zhou, Weilun Wang, Hezhen Hu, Hong Chen, and Houqiang Li. Dire for diffusion-generated image detection. *2023 IEEE/CVF International Conference on Computer Vision (ICCV)*, pages 22388–22398, 2023. 2, 3, 6, 7
- [37] Wukong, 2022. <https://xihe.mindspore.cn/modelzoo/wukong>. 6
- [38] Juncong Xu, Yang Yang, Han Fang, Honggu Liu, and Weiming Zhang. Famsec: A few-shot-sample-based general ai-generated image detection method. *IEEE Signal Processing Letters*, 2024. 3
- [39] Zhipei Xu, Xuanyu Zhang, Runyi Li, Zecheng Tang, Qing Huang, and Jian Zhang. Fakeshield: Explainable image forgery detection and localization via multi-modal large language models. *ArXiv*, abs/2410.02761, 2024. 3, 5
- [40] Nan Zhong, Yiran Xu, Zhenxing Qian, and Xinpeng Zhang. Rich and poor texture contrast: A simple yet effective approach for ai-generated image detection. *CoRR*, 2023. 3
- [41] Mingjian Zhu, Hanting Chen, Qiangyu Yan, Xudong Huang, Guanyu Lin, Wei Li, Zhijun Tu, Hailin Hu, Jie Hu, and Yunhe Wang. Genimage: A million-scale benchmark for detecting ai-generated image. *Advances in Neural Information Processing Systems*, 36:77771–77782, 2023. 2, 5, 6

A. Prompt Design

A.1. Flaw Classification Prompt

To generate the initial set of classified image flaws for constructing our GENEXPLAIN dataset, and then train a flaw classification model, we first prompted GPT-4o to classify these flaws, which were manually filtered afterwards.

Flaw Classification Guidelines for Synthetic Images

You will be provided with an AI generated image, try to identify systematic errors that make it distinguishable from natural real images from the categories below:

- 1. Lighting:** Unnatural or inconsistent light sources and shadows.
- 2. Color Saturation or Contrast:** Overly bright or dull colors, extreme contrasts disrupting image harmony.
- 3. Perspective:** Spatial disorientation caused by unrealistic angles or viewpoints, otherwise dimensionality errors such as flattened 3D objects.
- 4. Bad Anatomy:** For living creatures, mismatches and errors of body parts in humans or animals.
- 5. Distorted Objects:** For nonliving objects only, warped objects with fallacious details deviating from expected forms.
- 6. Structural Composition:** Poor positional arrangement between multiple elements in the scene.
- 7. Incomprehensible Text:** Malformed and unrecognizable text.
- 8. Implausible Scenarios:** Inappropriate behavior and situations unlikely to happen based on sociocultural concerns, or contradicting to historical facts.
- 9. Physical Law Violations:** Improbable physics, such as erroneous reflections or objects defying gravity.

Only select the categories below when highly confident:

- 10. Blurry or Inconsistent Borders:** Unclear or abrupt border outlines between elements.
- 11. Background:** Poorly blended or monotonous drab backgrounds.
- 12. Texture:** For nonliving objects only, significantly over-polished or unnatural textural appearances.
- 13. Generation Failures:** Major prominent rendering glitches or incomplete objects disrupting the entire scene.

If NONE of the categories above match, select:

14. Not Evident

Choose one or more categories above, and only reply the indexes of identified errors separated with commas, e.g. "1,3,6" for an image with "Lighting, Perspective, Structural Composition" errors, with no additional explanation.

PLEASE NOTE: Responses MUST be in the format of "[Number 1],[Number 2],..." (numbers and commas only) ordered from low to high, or "14" if no evident errors are found.

A.2. Initial Explanation Generation Prompt

After manually removing images with flaws that were incorrectly categorized, we prompted GPT-4o-mini to generate an initial explanation based on the description of the identified flaw.

Initial Explanation Generation Guidelines

You will be provided with an AI generated image confirmed with the following systematic error: <DESCRIPTION OF ERROR CATEGORY>

Give an explanation for why such an error is found in the image, and point out the specific location or items causing the error. Pay close attention to image details.

PLEASE NOTE: Responses should be concise, and organized into a SINGLE PARAGRAPH.

A.3. Iterative Explanation Refinement Prompt

For 3 rounds we iteratively refined the initial explanation and follow-ups. During each iteration, we calculated the Top-10 similar noun phrases with the synthetic image, and prompted GPT-4o-mini to retain these relevant phrases while additionally searching for overlooked flaws. The final refined explanations were added to our dataset.

Iterative Explanation Refinement Guidelines

You will be provided with an AI generated image confirmed with <ERROR CATEGORY> error. Below is an explanation of why this error appears in the image: <PREVIOUS EXPLANATION>

In this explanation, the following words may be highly relevant and accurately describe the image: <TOP 10 SIMILARITY PHRASES>

Your task is to refine the explanation to better align with the error in the image while retaining the relevant words. You can also analyze the image to identify whether any other potential errors that may have been overlooked about <ERROR CATEGORY>. Keep the explanation concise and avoid redundancy.

PLEASE NOTE: Responses should be concise, and organized into a SINGLE PARAGRAPH.